

Semi-Permeable Organic-Inorganic Hybrid Microreactors for Highly Efficient and Size-Selective Asymmetric Catalysis

Xiaoming Zhang, Lingyan Jing, Lijuan Wei, Fengwei Zhang, and Hengquan Yang

ACS Catal., Just Accepted Manuscript • DOI: 10.1021/acscatal.7b01659 • Publication Date (Web): 24 Aug 2017

Downloaded from <http://pubs.acs.org> on August 24, 2017

Just Accepted

“Just Accepted” manuscripts have been peer-reviewed and accepted for publication. They are posted online prior to technical editing, formatting for publication and author proofing. The American Chemical Society provides “Just Accepted” as a free service to the research community to expedite the dissemination of scientific material as soon as possible after acceptance. “Just Accepted” manuscripts appear in full in PDF format accompanied by an HTML abstract. “Just Accepted” manuscripts have been fully peer reviewed, but should not be considered the official version of record. They are accessible to all readers and citable by the Digital Object Identifier (DOI®). “Just Accepted” is an optional service offered to authors. Therefore, the “Just Accepted” Web site may not include all articles that will be published in the journal. After a manuscript is technically edited and formatted, it will be removed from the “Just Accepted” Web site and published as an ASAP article. Note that technical editing may introduce minor changes to the manuscript text and/or graphics which could affect content, and all legal disclaimers and ethical guidelines that apply to the journal pertain. ACS cannot be held responsible for errors or consequences arising from the use of information contained in these “Just Accepted” manuscripts.



Semi-Permeable Organic-Inorganic Hybrid Microreactors for Highly Efficient and Size-Selective Asymmetric Catalysis

Xiaoming Zhang,^{†#} Lingyan Jing,^{†#} Lijuan Wei,[†] Fengwei Zhang,[‡] Hengquan Yang^{*†}

[†]School of Chemistry and Chemical Engineering, Shanxi University, Taiyuan 030006, China

[‡]Institute of Crystalline Materials, Shanxi University, Wucheng Road 92, Taiyuan 030006, China

Supporting Information

ABSTRACT: A highly efficient and size-selective organic-inorganic hybrid microreactor was fabricated successfully by assembling the semi-permeable microporous silica hollow nanospheres at the interface of organic polymers containing an asymmetric transfer hydrogenation catalyst. The small micropores in the silica shells (1.0–1.5 nm) of the microreactors provide short mass-transfer channels for small molecules, but prevent the diffusion of large reactants through the shell. At the same time, the combination of the outer microporous silica and inner polymers endow the microreactor with hydrophobic/hydrophilic property, which helps its dispersion in water as well as the adsorption of reactant molecules from water, yielding an ideal microenvironment for water medium catalysis reactions. Such microreactors could efficiently catalyze the aqueous asymmetric transfer hydrogenation (ATH) of small-sized ketones with catalytic activity comparable to the homogeneous Rh-VBSPEN catalyst (TOF 625 vs 724 h⁻¹). Meanwhile, the microreactors also showed size selectivity toward large-sized reactants. Our studies provide an approach for the construction of artificial bio-inspired microreactors with size-selective properties and favorable catalysis microenvironments.

KEYWORDS: *bioreactor mimicking; hybrid microreactors; semi-permeable; size-selective; heterogeneous asymmetric catalysis*

INTRODUCTION

The cellular environment can be regarded as a sophisticated reaction locus, where metabolic pathways take place with unsurpassed efficiency and specificity. As a long-standing goal of bio-synthetic chemistry, the construction of assemblies that mimic the superior qualities of natural cells is highly desirable.^{1–4} These qualities often include the ability to operate in an aqueous solution at a near physiological pH, to provide a well-defined compartment for spatially isolated catalytic cycles and to select one substrate in light of its size or shape from a pool of structurally related molecules. Chemists have been trying to mimic them by selective encapsulation of catalysts in artificial microreactors.^{5–8} Enzymes, homogeneous metal catalysts and organocatalysts have been loaded into lipid vesicles, dendrimers, supramolecular architectures, sol-gel materials or silica scaffolds for various purposes.^{9–16} Although these techniques were successfully applied, the resultant solid catalysts often show decreased reactivity and selectivity compared to their homogeneous counterparts due to the altered microenvironment of the

active catalysts, diffusion barriers caused by the structure of solid support or low affinity of the solid surface to organic reactants. Accordingly, it is highly desirable to develop an efficient encapsulation method that not only provides an encapsulated catalyst which is compatible with homogeneous catalysts but also makes use of the positive effects of solid supports such as pore confinement effect or enrichment effect etc.

On the other hand, the size or shape-selective ability, which is an important and basic concept in the bio-synthetic system, is seldom achieved in the reported artificial microreactors so far.^{17–20} Such a concept is widely adopted in nature as most enzymes can highly selectively convert the right molecules that match their active sites in size or shape. Though shape- or size-selective catalysis phenomenon was already found in microporous zeolites or MOFs materials, and even used in chemical industry, the design of artificial microreactors possessing size or shape-selective properties while maintaining favorable reaction microenvironments still remains a challenge due to the inherent limitations of traditional mimicking methods.^{21–24}

A

Colloidosomes, which are usually formed by the self-assembly of nanoparticles at the immiscible liquid-liquid or gas-liquid interface during emulsification, have exhibited great promise in the development of artificial bio-microreactors.²⁵⁻³² Such synthetic capsules inherit the characteristics of emulsions, including bi-phase nature, compartmentalization effects, large surface area and remarkable interfacial stability. Active ingredients such as drugs, proteins, gas bubbles, catalyst or even living cells could be encapsulated into the colloidosome capsules easily through in situ processes.³³⁻⁴² And, the isolated inner space provides pretty good chances for the design of reaction microenvironment. It has also been found that the large interface area of colloidosome microcapsules facilitates the phase transfer of molecules across the interface, and can improve interfacial reaction efficiency by several orders of magnitude compared to bulk systems.⁴³⁻⁴⁵ Moreover, the spontaneous partitioning of colloidal particles at liquid-liquid or gas-liquid interfaces produces shell-like micro-structures. And by applying certain nanoparticles, microcapsules with semi-permeable-membrane-bound could be fabricated.^{20, 46, 47} Owing to these unique properties, colloidosome microcapsules have great potential as new robust microreactors with desired catalytic microenvironment and size-selective properties.

In this work, we describe an organic-inorganic hybrid colloidosome microcapsule with semi-permeability and ideal interior microenvironments as efficient microreactor for asymmetric catalysis. The capsules are composed of a shell made up with closely-packed size-sieving inorganic silica colloidal particles and inner organic macromolecular polymer layer with asymmetric catalyst in the frameworks. Controlled permeability of the shells of microcapsules enables size-selective catalysis and the interior organic layer endows the catalytic active sites with desired microenvironments. Moreover, the unique hybrid structure ensures long-term retention of the catalysts during catalytic cycles as well as the rapid diffusion of substrates and products into and out of microreactors. The hydrophobic polymers in the hydrophilic silica layer might induce a core-shell structure with hydrophobic polymer as a core and hydrophilic silica as a shell. Such a unique structure has been demonstrated to benefit aqueous reactions since the hydrophilic surface enables the particles to be well dispersed in water, while the hydrophobic core helps to absorb organic molecules from the surrounding aqueous environment.⁴⁸⁻⁵¹ As a proof of this concept, we use the aqueous asymmetric transfer hydrogenation (ATH) reaction catalyzed by Noyori-Ikariya catalyst (Rh, Ru or Ir complexes of TsDPEN) as a model to investigate the availability of colloidosome microcapsule platform. Our results demonstrated convincingly that the organic-inorganic microcapsule could be utilized as efficient fast-acting and size-selective microreactors.

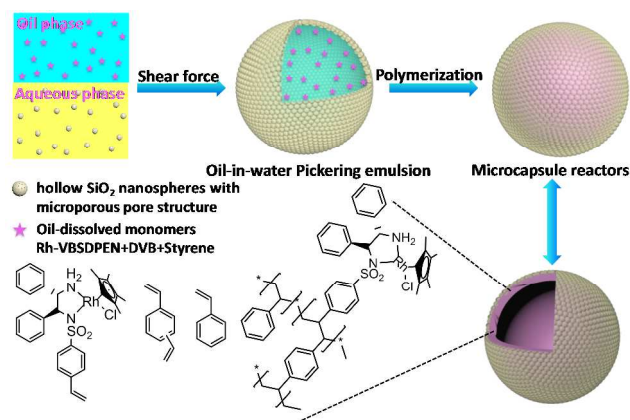


Figure 1. Schematic illustration of the preparation of semi-permeable organic-inorganic hybrid microreactors with a Pickering emulsion polymerization method.

RESULTS AND DISCUSSION

Formation and Characterization of Semi-permeable Organic-Inorganic Hybrid Microreactor

The semi-permeable organic-inorganic hybrid microreactors were prepared through a Pickering emulsion polymerization method, as illustrated in Figure 1. The whole process comprises two steps. First, an oil-in-water (o/w) Pickering emulsion is formulated by vigorously stirring a mixture of organic phase and aqueous suspension of solid emulsifier. During this process, hollow silica nanosphere that was synthesized through a single micelle template method was chosen as an emulsifier based on the following considerations.⁵²⁻⁵³ Such nanospheres possess a small particle size in the range of 20-30 nm and a hollow nanostructure with a ultra-thin shell (TEM, Figure 2a), which might be beneficial for the diffusion of molecules. Abundant micropores with dimension of 1.0 to 1.5 nm or even smaller are present on the shell (N₂ sorption and pore size distribution, Figure 3c, d), thereby providing an excellent test system to examine the effect of micropores on the retention or diffusion of molecules. Furthermore, the hollow nanosphere has hydrophilic surface properties (water contact angle 29°, Figure S1a), which is favorable for formation of an oil-in-water Pickering emulsion.⁵⁴ As shown in Figure S1b, after screening compositions, the Pickering emulsion was formulated with octanol as oil phase and aqueous suspension of silica hollow nanospheres as continuous phase. The oil phase contained a given amount of styrene (Sty) and divinylbenzene (DVB) monomers and initiator necessary to form cross-linked polymers. The hydrophobic catalyst, Rh-VBSPEN, was *in situ* encapsulated into the polymersomes by dissolving it into the octanol oil phase. The mass ratio of silica nanospheres to organics (octanol + Sty + DVB + Rh-VBSPEN) in the system is 1:5.92, and this mixture was sheared at 28500 rpm for 2 min to form a hollow silica nanosphere-stabilized emulsion. In this proportion, the amount of interfacial nanoparticles is much higher than

usual cases for achieving a full coverage of the droplets. The optical microscope image of emulsion droplets is shown in Figure S1c. Evidently, the resulting emulsion droplets are spherical in morphology, and polydisperse in size. The formed Pickering emulsions were sufficiently stable against coalescence without visible separation of the dispersed phase after standing for 3 d, which is important for the following polymerization step. In the second step, the monomers dissolved in the oil phase polymerized and formed polymer@silica composites upon thermal annealing the Pickering system at 70 °C for 20 h. After polymerization, the composite was washed with a series of ethanol/water solvents and dried under vacuum, the assembled “colloidosomes” were structurally reinforced into robust free-standing capsules. As shown in Figure S1d, the microcapsule structure could still be maintained intactly even in the presence of a demulsification reagent ethanol. The morphology and size of the capsules are similar to those of the initial Pickering emulsion droplets, confirming that the microreactors are originated from precursor emulsion droplets.

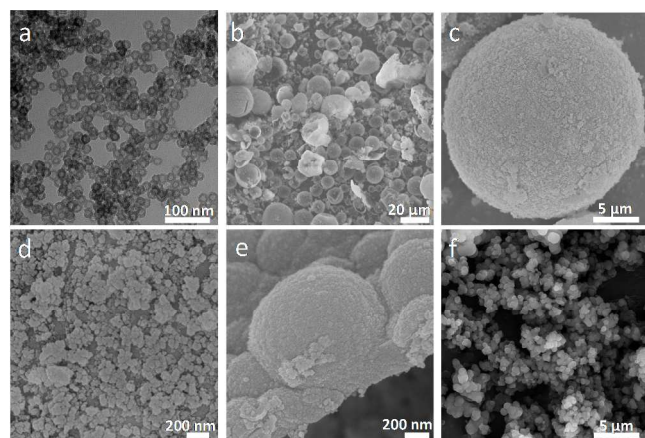


Figure 2. (a) TEM image of hollow silica nanospheres; (b) SEM image of organic-inorganic hybrid microcapsules; (c) magnification of a hybrid microcapsule showing the spherical structures; (d) the densely packed out-layer; (e) a broken microcapsule revealing the hollow interior and inner surface structure and (f) polymer nanoparticles without the formation of Pickering emulsion aisle.

Scanning electron microscope (SEM) images of the hybrid microcapsules reveal the formation of individual intact spherical structures with a size distribution of $20 \pm 12 \mu\text{m}$, together with few broken spheres (Figure 2b). Most of the microspheres are stable under the working conditions of the SEM analysis, suggesting moderate mechanical stability. The size of the hybrid spheres is polydispersed, which may be due to the emulsification process. The image of hybrid hollow spheres is shown in Figure 2c, which clearly shows the spherical structures and the presence of silica building blocks on the surface of the capsules. Under a higher magnification (Figure 2d), silica hollow nanospheres are observed to be randomly

distributed over the surface of these microspheres, completely covering its surface, indicating that the as-made silica hollow nanosphere is sufficiently wettable by the dispersed oil phase without further modification that is often required to generate stable emulsions from inorganic colloids. This dense over-layer renders the capsules with additional structural stability, and strongly suggests these could be utilized in size-selective applications where molecular access is controlled by the highly regular micropores of the silica hollow nanospheres as previously reported for catalysis by encapsulating noble metal NPs.⁵⁵ Figure 2e shows that the obtained hybrid spheres are hollow structured, small nanospheres are found in the inner surface of the wall, which might be a result of phase separation of the polymer during polymerization as octanol chosen is a poor solvent for the cross-linked polymer network, leading to phase separation and precipitation at the interface and thus locking the silica nanospheres into the capsule surface. The nature of the oil phase is very important for the formation of hollow structure. For example, replacing octanol with a good swelling reagent towards organic polymers, like toluene, yields core-shell structures under the same reaction conditions (Figure S2). This is due to the fact that toluene can swell the polymer network preventing effective phase separation for the formation of hollow capsule. Polymer nanoparticles with particle size of 500–600 nm could also be obtained without the formation of Pickering emulsion aisle (Figure 2f). However, such polymer catalyst doesn't possess the unique hollow structure and densely packed silica shell.

The organic-inorganic microreactors were further characterized by FT-IR, thermogravimetric analysis (TGA) and nitrogen adsorption. FT-IR was applied to verify the composition of the hollow microcapsules. As shown in Figure 3a, the characteristic bands from silica can be observed at around 3447, 1631, and 1104 cm^{-1} respectively for ν (O–H), δ (O–H), and ω (Si–O) in the spectra of hybrid capsules. The bands around 2858–3061 cm^{-1} , 1418–1510 cm^{-1} and 678–750 cm^{-1} that are assigned to the C–H stretching vibrations, the C=C vibrations and breathing vibrations of the phenyl ring are also observed, suggesting the successful incorporation of polymers in the microcapsules. The organic group content and thermal stability of capsules was investigated using the thermogravimetric analysis (TGA) technique (Figure 3b). The capsules largely decompose in a single step in the temperature range of 340–500 °C, and a small step is also observed between 500–650 °C. The polymer contents is determined to be 45 wt% on the basis of the weight loss after full decomposition. Nitrogen adsorption isotherms at 77 K demonstrate that the capsules are porous with an apparent BET surface area of 112 m^2/g and a pore volume of 0.989 cm^3/g . Its isotherm is distinct from that of pure silica hollow nanospheres, reflecting the overall contribution of the polymer component. DFT pore size distribution analysis reveals that abundant micropores existed in the microcapsules, with size similar with the

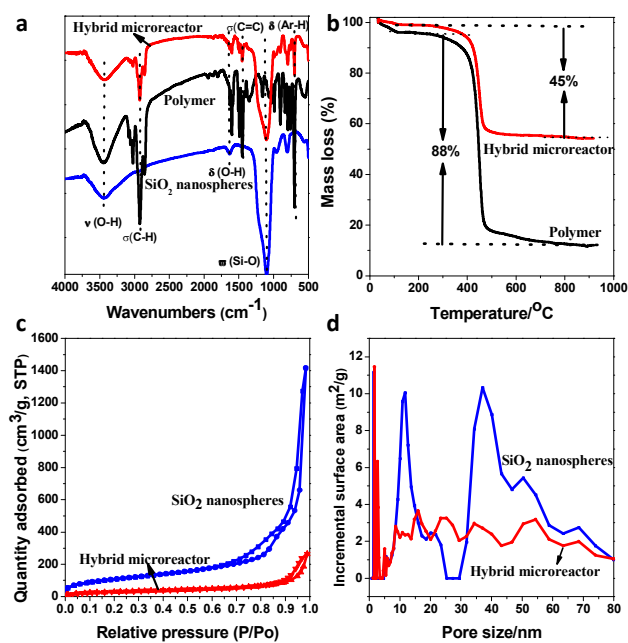


Figure 3. (a) FT-IR spectra of SiO₂ hollow nanosphere, polymer and hybrid microreactor; (b) TG of hybrid microreactor and polymer; (c) nitrogen adsorption-desorption isotherm and (d) pore size distributions calculated from the adsorption branches using a nonlocal density functional theory (NLDFT) method of the hollow silica nanospheres and hybrid microreactors.

interfacial silica nanospheres, demonstrating that the pores of silica nanospheres remain accessible in the composite capsules. The mesopores corresponding to the hollow cavity of the silica nanospheres was disappeared, which might be attributed to the filling by polymers.

Shell Permeability and Interior Microenvironment

The permeability of the microreactor shell is critical for their potential in size-selective applications, and here we used fluorescent dyes to visualize the molecular uptake and release. As an effective probe of shell permeability, the probe molecule should ideally be inaccessible to the silica micropores. Therefore, we firstly selected a large water soluble dye, fluorescein isothiocyanate (see in Figure S3, FITC, 1.0*0.9*0.7 nm³, considering the solvation effect, the actual size of a moving molecule might be larger than the theoretical molecular size obtained from the calculation), to assess the reactor permeability. By immersing the synthesized microcapsules in the dye solution, the diffusion ability of FITC from the bulk solution to the interior was investigated. After washing with water several times, fluorescence confocal microscopy image (CLSM) was recorded. As shown in Figure 4a, CLSM image show that the interior and shell of the capsules remain almost totally dark, suggesting that the large dye molecule can't diffuse through the dense-packed microporous silica hollow nanosphere layer into the interior of the capsule. This also confirms the

important role of the semi-permeable shell structure, since FITC, as an organic molecule, tends to be adsorbed by the inner polymer component due to interactions between the abundant organic functionalities of the hybrid framework particles and the aromatic dye. On the other hand, oil soluble Nile Red with molecular size of 1.4 nm*0.6 nm was loaded into the capsules by *in situ* dissolving a small amount of such fluorescent dye in the octanol phase of interfacial active silica-stabilized Pickering emulsions during synthesis. After polymerization and washing with EtOH to remove non-encapsulated dyes, the capsules were re-dispersed in EtOH to assess the dye release. As shown in Figure 4b, the Nile Red is observed in the capsules and mainly concentrated around and/or within the interior of the capsule shell as evidenced by the observed red halo, which is consistent with a strong interaction between the shell and the dye, since polymers are distributed in the inner surface of the capsules. Notably, no dye molecules were observed in the continuous ethanol solution, demonstrating the successful encapsulation of the fluorescent dye molecules and the high accumulation ability of the interior of the capsule shells to the organic dyes. Such a result also indicates that the small micropores of silica shell component can regulate dye access through the porous polymer shell into the external medium.

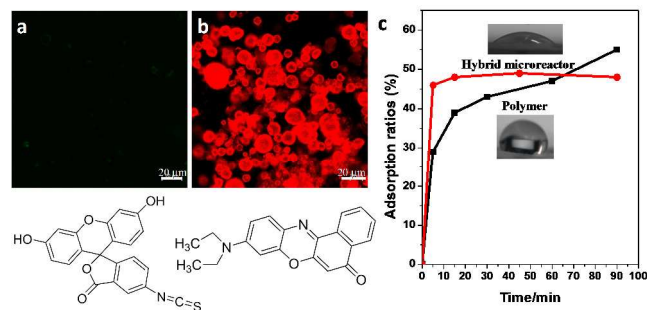


Figure 4. Shell permeability properties of hybrid microreactors. (a) CLSM image of microreactors after soaking in FITC solution; (b) CLSM image of microreactors loaded with Nile Red; (c) time vs. adsorption curves of hybrid microreactors and polymer towards aqueous solution of *p*-aminophenol.

For further investigating the permeability of the porous shell, a water soluble small molecule *p*-aminophenol was also selected to assess the adsorption capacity of these microcapsules. According to the adsorption test in Figure 4c, the organic-inorganic microporous capsules could efficiently adsorb *p*-aminophenol from the aqueous surroundings, and exhibited a faster adsorption rate than the pure polymers, which could be attributed to the unique polymer@silica hollow structures. The hydrophilic silica nanoparticles at the interface confer the hydrophilicity to the microcapsule surface (water contact angle 30°) for its good dispersion in water, while the interior hydrophobic polymer (water contact angle 100°)

endows the capsules with good ability to absorb organic molecules. The good dispersibility in water also shortens the diffusion distance and benefits the adsorption. Furthermore, the hydrophobic@hydrophilic structures provide the unique microenvironment of the interior catalyst. The final saturated adsorption capacity is a little lower than the polymers, due to the lower organic group contents. This adsorption test indicates the good permeability of the shell to small molecules and enrichment effects towards organic substrates in water.

The Size-Selective Asymmetric Transfer Hydrogenation Reactions

As a type of highly active and enantioselective catalysts, the chiral N-sulfonylated diamine-based organometallic catalysts have been studied extensively in the aqueous asymmetric transfer hydrogenation (ATH) of aromatic ketones.⁵⁶⁻⁶⁰ And due to the advantages of the high catalytic performance of the reaction system, operational simplicity, safety, and the easy availability of reductants, this reaction is promising for practical applications. For a heterogeneous catalytic process, focuses are mainly concentrated on the development of highly active solid catalyst or cascade reaction systems, seldom reports can be found about the size-selective catalysis.⁶¹⁻⁶³ Here, with the valuable semi-permeable microcapsule solid catalyst in hand, we examined systemically their size-selectively catalytic activities and enantioselectivities.

Since the molecular size of hydrogen source HCOONa is so small that the size effects can be negligible, and the size-selectivity could be explored with different aromatic ketones. Here, we chose three different sized compounds, including acetophenone, 1-acetylnaphthalene and 3, 5-dibenzoyloxyacetophenone, as substrates to assess the catalytic performance of semi-permeable organic-inorganic hybrid microreactors and their size-selectivity. For comparison, the pure polymer catalyst without shell structure and homogeneous Rh-VBSPEN were also evaluated. The reactions were carried out at 40 °C in water, and monitored by GC or HPLC with a chiral column. As shown in Table 1 (entry 1), for the small substrate acetophenone, the solid microcapsule catalyst could smoothly catalyze the reaction with a 98% conversion and 95% ee within 1.5 h, which is almost the same as its corresponding homogeneous Rh-VBSPEN catalyst (entry 2). This indicates that the activity of complex catalyst is maintained after being incorporated into the hybrid microcapsules and also suggests that acetophenone as small reactant can readily diffuse through the framework micropores of the outer shell. However, under the identical reaction conditions, the polymer catalyst gives only 86% conversion and 94% ee using cetyltrimethylammonium bromide (CTAB) a phase transfer reagent during the reaction (entry 3). The lower activity might be related to its nonporous structure and hydrophobic surface properties, which are not beneficial for the exposure of active site and for mass transport in aqueous solution.

To further evaluate the high activity of hybrid microcapsule catalyst, the dependences of acetophenone conversion on reaction time over the microcapsule catalyst and its homogeneous counterpart are compared, as shown in Figure 5a. Notably, the solid microcapsule catalyst exhibited a comparable reaction rate with the homogeneous Rh-VBSPEN catalyst, while the polymer catalyst showed relatively lower efficiency. After normalization, as shown in Figure 5d, the hybrid microreactor catalyst affords a turnover frequency (TOF) of 625 h⁻¹, which approaches that for the homogeneous catalyst (724 h⁻¹) and 1.4 times higher than that for the polymer catalyst (449 h⁻¹). These comparisons demonstrate that the encapsulated polymer-based-catalyst is as active as the homogeneous counterpart. The high activity might be attributed to its unique microstructures. On one hand, the catalyst features a hydrophobic polymer core and a hydrophilic silica shell. The hydrophilic shell would ensure good dispersion of the solid catalyst in water and benefits the contact with water dissolved hydrogen source HCOONa. The hydrophobic inner would provide desired microenvironment for the catalysis and drive the adsorption of organic reactants from water. The kinetic barriers caused by the access of organic substrates to catalytically active sites would be thus alleviated. Such a phenomenon has also been observed in other catalytic systems, such as carbon nanotube, amphiphilic polymer, and superhydrophobic catalyst.^{51,64,65} On the other hand, the nanometer-sized shells with short, unhindered microchannels might also favor the mass-transfer, and improve the catalytic performance. To verify this advantage, adsorption test of an amphipathic molecule *p*-aminophenol was performed (Figure 4c). The solid microreactor could quickly enrich the adsorbate from its aqueous solution, and has a high adsorption capacity.

An important feature of the hybrid microreactor catalyst is the ease of separation by simple centrifugation while retaining its catalytic activity and enantioselectivity after multiple cycles of use. As shown in Figure 6, the hybrid solid microreactors could be recycled over five consecutive reactions, while the ee values and conversions were well maintained despite longer reaction times. Since the textural parameters and polymer content remain almost the same as the fresh solid catalyst (see N₂ sorption and TG measurements of recycled catalyst, in Figure S4), the decreased activity was unlikely related to the textural parameters or loss of polymer unit. To further reveal the deactivation reasons, ICP analysis was also performed, which shows 6.8% of Rh loading in total was leached. However, such a low metal leaching amount was not enough to account for the decreased activity. The decreased activity might be relevant to the deterioration of active chiral catalysts caused by their decomposition under reaction conditions.^{59,60,66}

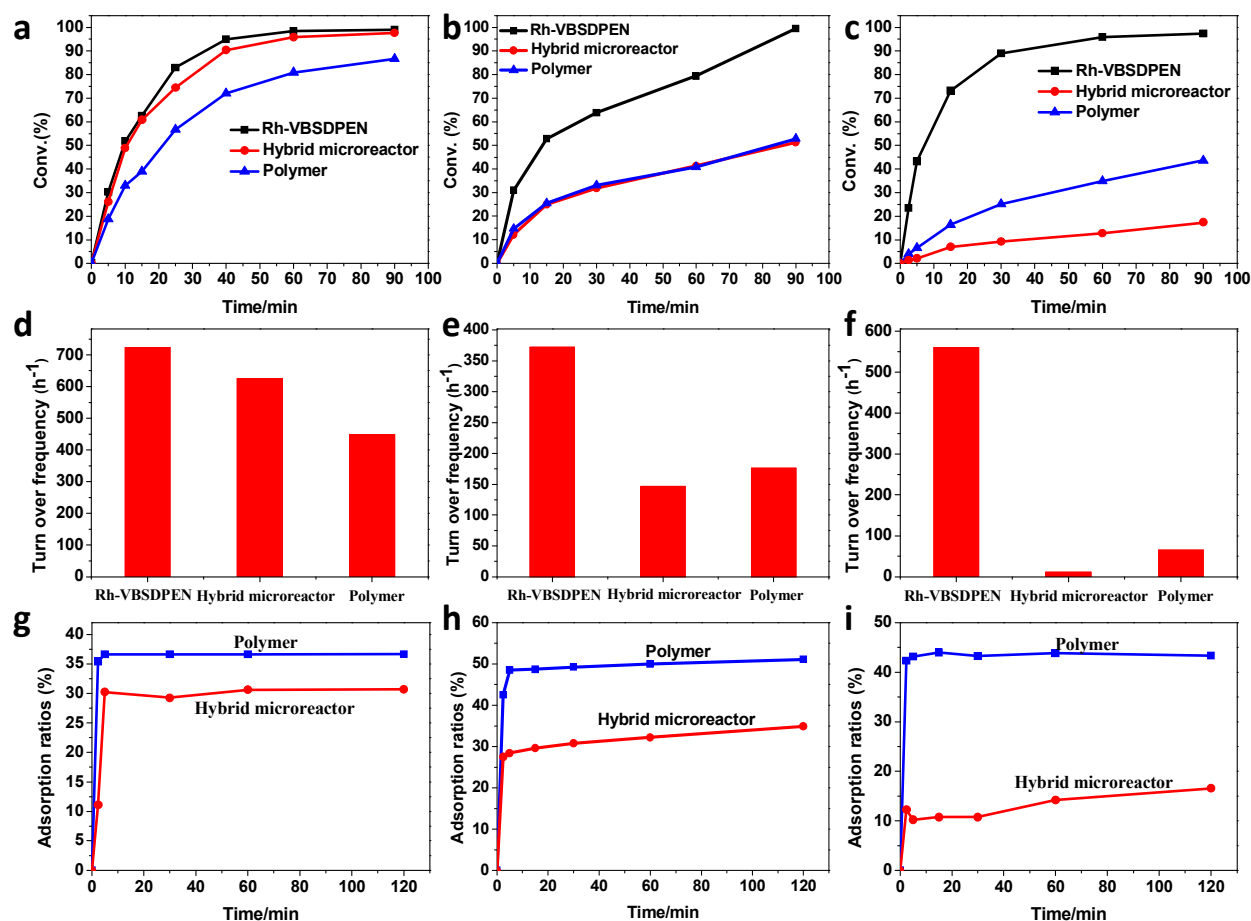


Figure 5. Kinetic plots of asymmetric transfer hydrogenation of acetophenone (a), 1-acetylnaphthalene (b) and 3, 5-dibenzoyloxyacetophenone (c) catalyzed by different catalysts (homogeneous catalyst, black; microcapsule solid catalyst, red; polymer catalyst, blue); turn over frequencies (TOFs) for different catalysts with different substrates, acetophenone (d), 1-acetylnaphthalene (e) and 3, 5-dibenzoyloxyacetophenone (f); time vs adsorption curves of hybrid microcapsules and polymer towards aqueous solution of different substrates, acetophenone (g), 1-acetylnaphthalene (h) and 3, 5-dibenzoyloxyacetophenone (i), the total dosages of acetophenone, 1-acetylnaphthalene and 3, 5-dibenzoyloxyacetophenone were 60 mg, 42 mg and 42 mg, respectively and the absorbents were 50 mg (see SI, experimental section).

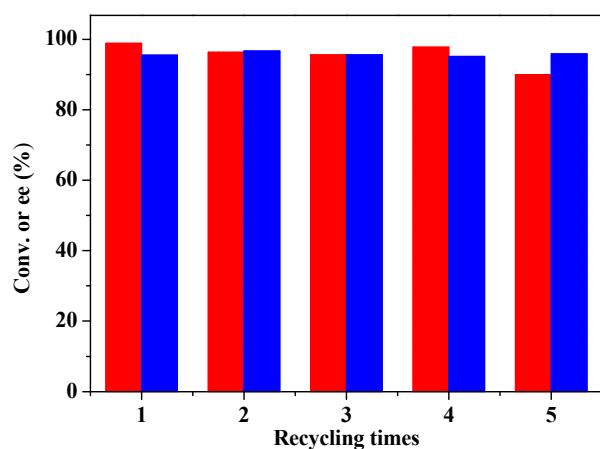


Figure 6. Recyclability of the hybrid microreactor catalyst in the asymmetric transfer hydrogenation of acetophenone (the reaction time for cycles 1, 2, 3, 4 and 5 is 1.5 h, 3 h, 8 h, 12 h, and 16 h, respectively).

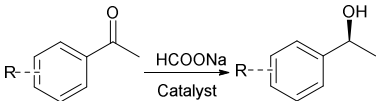
ATH of 1-acetylnaphthalene over the homogeneous Rh-VBSPDEN was similar to that observed for acetophenone, reaching a full conversion after 1.5 h (Figure 5b). In this case, however, much lower activity was found over the hybrid microcapsule catalyst and only 51% of conversion could be obtained, which is similar to the polymer catalyst (TOF 146 vs 176 h⁻¹, Figure 5e). Interestingly, when a larger compound 3, 5-dibenzoyloxyacetophenone was utilized as the substrate, much lower conversion was achieved with the hybrid microcapsule catalyst (about 17%, Figure 5c). This activity is even lower than that of the pure polymer catalyst, with which 43% of final conversion could be obtained within the same reaction time. After normalization, as shown in Figure 5f, the hybrid microcapsule catalyst only affords a TOF of only 11 h⁻¹. In comparison, 561 h⁻¹ and 65 h⁻¹ of TOF values could be obtained with the homogeneous Rh-VBSPDEN and pure polymer catalysts. So, the activity of these catalysts is in the order of Rh-VBSPDEN > polymer > hybrid microreactor catalyst. However, the trend of conversions

and TOF over these catalysts is very different from the small substrate (acetophenone) and moderate sized 1-acetylnaphthalene. These results suggest a size-selective catalytic process, which might be attributed to the variation in molecular size of the substrates and the semi-permeability of the microporous shell to regulate their access. To solidify this conclusion, the molecular sizes of these investigated molecules were calculated. Based on the optimized geometries, the sizes of acetophenone, 1-acetylnaphthalene and 3, 5-dibenzoyloxyacetophenone were estimated to be 0.68 nm*0.499 nm, 0.81*0.68 nm and 1.6 nm*1.4 nm (see in Figure S3), respectively. Apparently, 3, 5-dibenzoyloxyacetophenone is much larger than the former substrates. The size of acetophenone is smaller than the aperture size of silica shell, and these molecules could pass through the micropores of the dense packed silica outer layer to access the microreactor interior. As the molecular size increases, the diffusion resistance exacerbates, resulting in decreased catalytic activity with 1-acetylnaphthalene. For the larger molecule 3, 5-dibenzoyloxyacetophenone, the size is nearly equal to the pore size, so it is expected to be excluded by the micropores of the reactor shell, resulting significantly increased diffusion barrier stemming from the potential blockage of pores. It is likely that the large substrate pass through the defects within the outer layer, which is responsible for the observed albeit very low activity. To further reveal the size-selective-ability, the catalytic performance of the microcapsule catalyst in asymmetric transfer hydrogenation of a mixture of acetophenone and 3, 5-dibenzoyloxyacetophenone was also examined. As shown in Figure S5, under the same reaction conditions, small substrate acetophenone could be smoothly converted to desired chiral aromatic alcohol with a conversion as high as 96%, while only 8.3% of conversion was obtained for 3, 5-dibenzoyloxyacetophenone, further confirming the size-selectivity of the microcapsule reactors.

The size-selective effects of the microreactors were also further confirmed by the adsorption tests. Different sized substrates were examined, as shown in Figure 5g and 5h, the microcapsule catalyst has a strong adsorption capacity (calculated to be 368 and 293 mg/g) for small substrate acetophenone and 1-acetylnaphthalene, while a small quantity of the large substrate 3, 5-dibenzoyloxyacetophenone was adsorbed (Figure 5i, about 55 mg/g). This result further demonstrates the increased blockage barrier of microreactors towards larger molecule. Compared with the hybrid microcapsule material, the polymer exhibited higher and faster adsorption rate due to its good wettability to organics. However, due to the hydrophobic properties, water soluble hydrogen source might be not easy to access the polymer framework. Although size-selective catalysis has been reported with MOFs or zeolites structures, this work provides an alternative strategy for the formation of size-selective solid asymmetric catalysts, since polymerization is one of

the most common and mature immobilization strategies.⁶⁷

Table 1 Asymmetric transfer hydrogenation of ketones catalyzed by microreactor catalyst^a



Entry	Reaction time (h)	Substrates	Conv. (%) ^b	Ee (%) ^b
1	1.5	H	98	95
2 ^c	1.5	H	>99	95
3 ^d	1.5	H	86	94
4	1.5	4-F	>99	94
5	1.5	4-Cl	>99	94
6	1.5	4-Br	>99	94
7	1.5	4-Me	98	93
8	1.5	4-OMe	79	95
9	1.5	3-F	>99	94
10	1.5	3-Br	>99	94
11	1.5	3-Me	90	91
12	1.5	4- <i>i</i> -Bu	39	95
13	5	4- <i>i</i> -Bu	95	95

^a Reaction conditions: solid catalyst (2.5 μmol Rh), HCOONa (0.17 g, 2.5 mmol), ketones (0.5 mmol) and 2.0 ml H₂O, reaction temperature (313 K). ^b Analysis by GC using a Agilent-113-2532 Cyclodex-B chiral column. ^c Homogeneous Rh-VBSPEN as catalyst. ^d Pure polymer catalyst with CTAB as phase transfer reagent.

Encouraged by the superior performance of hybrid microcapsule catalyst, other ketones have been intensively investigated (Table 1). The results show that various ketones are efficiently converted into chiral alcohols with high ee values (91-95%) using HCOONa as the reductant and water as the solvent. However, the reaction rates for different substrates vary considerably. For example, with electron-withdrawing substituent groups, including -F, -Cl, -Br, ketones can be converted completely within 1.5 h, but for electron-rich aromatic ketones with -CH₃ or -OCH₃ substituent groups, the activities are a little lower, and only 98 % and 79 % of conversions could be obtained within the same reaction time (entries 4-8). The position of the substituted groups also has significant influence on the reaction efficiency. With meta-substituted -F or -Br, ketones can be converted completely similarly (entries 9, 10). However, with meta-substituted -CH₃, only 90% of conversion could be got (entry 11). The decreased activity might also be related with its spatial size. To clarify this, a larger substituted group, *i*-Bu, was also investigated. Under identical reaction conditions, only 39% of conversion was obtained, much lower than other substrates (entry 12). Prolonging the reaction time to 5 h, a much higher

conversion, about 95%, could be got (entry 13). These results further demonstrate the efficiency of our solid catalyst and its size-selective properties.

CONCLUSION

In summary, we have developed an organic-inorganic hybrid microreactor possessing unique semi-permeable and hydrophobic@hydrophilic properties with encapsulated asymmetric homogeneous Noyori-Ikariya catalyst. The developed solid catalyst exhibited excellent catalytic performance (TOF 625 h⁻¹, 95% ee) in the asymmetric transfer hydrogenation of small aromatic ketones, demonstrating that the immobilization process did not compromise their catalytic performance, which might be attributed to the synergy of appropriate semi-permeable pore size and finely engineered hydrophobic microenvironment around the catalyst centers. Size-selective permeability of the capsule shell allows the creation of size-selective reactors. Substrates with large sizes did not show noticeable conversion, because of the significantly increased diffusion barrier stemming from the potential blockage of micropores. This method might be readily adaptable to a broad range of other catalysts and is appealing for the development of novel functional microscale ensembles that mimic bio-microreactors.

ASSOCIATED CONTENT

AUTHOR INFORMATION

Corresponding Author

*hgyang@sxu.edu.cn

Author Contributions

The manuscript was written through contributions of all authors. All authors have given approval to the final version of the manuscript. [#]These authors contributed equally.

Supporting Information

Experimental section; Appearance of the Pickering emulsion and its optical micrograph; SEM image; The molecular structure and size of fluorescent probes and reactant molecules; The N₂ sorption and TG measurements of recycled catalyst; The GC and HPLC traces for various substrates. This material is available free of charge via the Internet at <http://pubs.acs.org>.

ACKNOWLEDGMENT

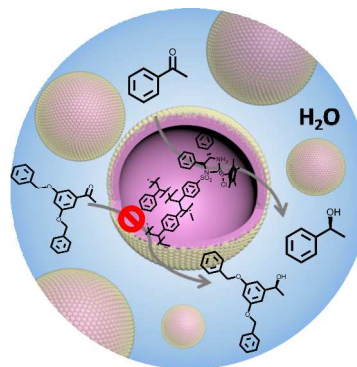
This work is supported by the Natural Science Foundation of China (21603128), the Natural Science Foundation for Young Scientists of Shanxi Province (2016021034), the Scientific Research Start-up Funds of Shanxi University (rsc723).

REFERENCES

1. Wang, Z. J.; Clary, K. N.; Bergman, R. G.; Raymond, K. N.; Toste, F. D. *Nat. Chem.* **2013**, 5, 100–103.
2. Marguet, M.; Bonduelle, C.; Lecommandoux, S. *Chem. Soc. Rev.* **2013**, 42, 512–529.
3. Oers, MCM V.; Rutjes, FPJT; Hest, JCM V. *Curr. Opin. Biotech.* **2014**, 28, 10–16.
4. Marguet, M.; Edembe, L.; Lecommandoux S. *Angew. Chem. Int. Ed.* **2012**, 51, 1173–1176.
5. Chi, Y. G.; Scroggins, S. T.; Frechet, J. M. J. *J. Am. Chem. Soc.* **2008**, 130, 6322–6323.
6. Bai, S. Y.; Yang, H. Q.; Wang, P.; Gao, J. S.; Li, B.; Yang, Q. H.; Li, C. *Chem. Commun.* **2010**, 46, 8145–8147.
7. Yang, Y.; Liu, X.; Li, X. B.; Zhao, J.; Bai, S. Y.; Liu, J.; Yang, Q. H. *Angew. Chem. Int. Ed.* **2012**, 51, 9164–9168.
8. Han, Q. X.; Qi, B.; Ren, W. M.; He, C.; Niu, J. Y.; Duan, C. Y. *Nat. Commun.* **2015**, 6, 10007.
9. Peters, R. J. R. W.; Marguet, M.; Marais, S.; Fraaije, M. W.; van Hest, J. C. M.; Lecommandoux, S. *Angew. Chem. Int. Ed.* **2014**, 53, 146–150.
10. Gorbe, T.; Gustafson, K. P. J.; Verho, O.; Kervefors, G.; Zheng, H. Q.; Zou, X. D.; Johnston, E. V.; Backvall, J. E. *ACS Catal.* **2017**, 7, 1601–1605.
11. Egi, M.; Sugiyama, K.; Saneto, M.; Hanada, R.; Kato, K.; Akai, S. *Angew. Chem. Int. Ed.* **2013**, 52, 3654–3658.
12. Wang, Z. P.; Van Oers, M. C. M.; Rutjes, F. P. J. T.; Van Hest, J. C. M. *Angew. Chem. Int. Ed.* **2012**, 51, 10746–10750.
13. Wang, W. L.; Zheng, A. M.; Zhao, P. Q.; Xia, C. G.; Li, F. W. *ACS Catal.* **2014**, 4, 321–327.
14. Tonga, G. Y.; Jeong, Y. D.; Duncan, B.; Mizuhara, T.; Mout, R.; Das, R.; Hou, S.; Rotello, V. M. *Nat. Chem.* **2015**, 7, 597–603.
15. Boyjoo, Y.; Wang, M. W.; Pareek, V. K.; Liu, J.; Jaroniec M. *Chem. Soc. Rev.* **2016**, 45, 6013–6047.
16. Yang, T. Y.; Ling, H. J.; Lamonier, J. F.; Jaroniec, M.; Huang, J.; Monteiro, M. J.; Liu, J. *NPG Asia Mater.* **2016**, 8, e240.
17. Liang, K.; Ricco, R.; Doherty, C. M.; Styles, J. M.; Bell, S.; Kirby, N.; Mudie, S.; Haylock, D.; Hill, A. J.; Doonan, C. J.; Falcaro, P. *Nat. Commun.* **2015**, 6, 7240.
18. Yang, H. Q.; Chong, Y. Z.; Li, X. K.; Ge, H.; Fan, W. B.; Wang, J. G. *J. Mater. Chem.* **2012**, 22, 9069–9076.
19. Yang, J.; Zhang, F. J.; Lu, H. Y.; Hong, X.; Jiang, H. L.; Wu, Y. E.; Li, Y. D. *Angew. Chem. Int. Ed.* **2015**, 54, 10889–10993.
20. Huo, J.; Aguilera-Sigalat, J.; El-Hankari, S.; Bradshaw, D. *Chem. Sci.* **2015**, 6, 1938–1943.
21. Cui, T. L.; Ke, W. Y.; Zhang, W. B.; Wang, H. H.; Li, X. H.; Chen, J. S. *Angew. Chem. Int. Ed.* **2016**, 55, 9178–9182.
22. Laursen, A. B.; Hojholt, K. T.; Lundegaard, L. F.; Simonsen, S. B.; Helveg, S.; Schuth, F.; Paul, M.; Grunwaldt, J. D.; Kegnoes, S.; Christensen, C. H.; Egeblad, K. *Angew. Chem. Int. Ed.* **2010**, 49, 3504–3507.
23. Zhang, W. N.; Lu, G.; Cui, C. L.; Liu, Y. Y.; Li, S. Z.; Yan, W. J.; Xing, C.; Chi, Y. R.; Yang, Y. H.; Huo, F. W. *Adv. Mater.* **2014**, 26, 4056–4060.
24. Liu, H. L.; Chang, L. N.; Bai, C. H.; Chen, L. Y.; Luque, R.; Li, Y. W. *Angew. Chem. Int. Ed.* **2016**, 55, 5019–5023.
25. Dinsmore, A. D.; Hsu, M. F.; Nikolaides, M. G.; Marquez, M.; Bausch, A. R.; Weitz, D. A. *Science* **2002**, 298, 1006–1009.
26. Pang, M. L.; Cairns, A. J.; Liu, Y. L.; Belmabkhout, Y.; Zeng, H. C.; Eddaoudi, M. *J. Am. Chem. Soc.* **2013**, 135, 10234–10237.
27. Park, J. I.; Nie, Z.; Kumachev, A.; Abdelrahman, A. I.; Binks, B. R.; Stone, H. A.; Kumacheva, E. *Angew. Chem. Int. Ed.* **2009**, 48, 5300–5304.
28. Sheng, Y. F.; Sun, G. Q.; Wu, J.; Ma, G. H.; Ngai, T. *Angew. Chem. Int. Ed.* **2015**, 54, 7012–7017.

29. Huang, J. P.; Cheng, F. Q.; Binks, B. P.; Yang, H. Q. *J. Am. Chem. Soc.* **2015**, 137, 15015–15025.
30. Potier, J.; Menuel, S.; Chambrier, M. H.; Burylo, L.; Blach, J. F.; Woisel, P.; Monflier, E.; Hapiot, F. *ACS Catal.* **2013**, 3, 1618–1621.
31. Vericella, J. J.; Baker, S. E.; Stolaroff, J. K.; Duoss, E. B.; Hardin, J. O.; Lewicki, J.; Glogowski, E.; Floyd, W. C.; Valdez, C. A.; Smith, W. L.; Satcher, J. H.; Bourcier, W. L.; Spadaccini, C. M.; Lewis, J. A.; Aines, R. D. *Nat. Commun.* **2015**, 6, 6124.
32. Xu, X. W.; Zhang, X. M.; Liu, C.; Yang, Y. L.; Liu, J. W.; Cong, H. P.; Dong, C. H.; Ren, X. F.; Yu, S. H. *J. Am. Chem. Soc.* **2013**, 135, 12928–12931.
33. Yang, H. Q.; Fu, L. M.; Wei, L. J.; Liang, J. F.; Binks, B. P. *J. Am. Chem. Soc.* **2015**, 137, 1362–1371.
34. Murakami, R.; Moriyama, H.; Yamamoto, M.; Binks, B. P.; Rocher, A. *Adv. Mater.* **2012**, 24, 767–771.
35. Huo, J.; Marcello, M.; Garai, A.; Bradshaw, D. *Adv. Mater.* **2013**, 25, 2717–2722.
36. Jeong, G. Y.; Ricco, R.; Liang, K.; Ludwig, J.; Kim, J. O.; Falcato, P.; Kim, D. P. *Chem. Mater.* **2015**, 27, 7903–7909.
37. Carne-Sanchez, A.; Imaz, I.; Cano-Sarabia, M.; Maspocho, D. *Nat. Chem.* **2013**, 5, 203–211.
38. Shi, J. F.; Wang, X. L.; Zhang, W. Y.; Jiang, Z. Y.; Liang, Y. P.; Zhu, Y. Y.; Zhang, C. H. *Adv. Funct. Mater.* **2013**, 23, 1450–1458.
39. Li, W. B.; Zhang, Y. F.; Xu, Z. H.; Meng, Q.; Fan, Z.; Ye, S. J.; Zhang, G. L. *Angew. Chem. Int. Ed.* **2016**, 55, 955–959.
40. Chen, Z. W.; Zhou, L.; Bing, W.; Zhang, Z. J.; Li, Z. H.; Ren, J. S.; Qu, X. G. *J. Am. Chem. Soc.* **2014**, 136, 7498–7504.
41. Chen, Z. W.; Ji, H. W.; Zhao, C. Q.; Ju, E. G.; Ren, J. S.; Qu, X. G. *Angew. Chem. Int. Ed.* **2015**, 54, 4904–4908.
42. Dewey, D. C.; Strulson, C. A.; Cacace, D. N.; Bevilacqua, P. C.; Keating, C. D. *Nat. Commun.* **2014**, 5, 4670.
43. Zhou, W. J.; Fang, L.; Fan, Z. Y.; Albela, B.; Bonneviot, L.; De Campo, F.; Pera-Titus, M.; Clacens, J. M. *J. Am. Chem. Soc.* **2014**, 136, 4869–4872.
44. Zhang, W. J.; Fu, L. M.; Yang, H. Q. *ChemSusChem* **2014**, 7, 391–396.
45. Zhang, M.; Wei, L. J.; Chen, H.; Du, Z. P.; Binks, B. P.; Yang, H. Q. *J. Am. Chem. Soc.* **2016**, 138, 10173–10183.
46. Li, M.; Harbron, R. L.; Weaver, J. V. M.; Binks, B. P.; Mann, S. *Nat. Chem.* **2013**, 5, 529–536.
47. Ameloot, R.; Vermoortele, F.; Vanhove, W.; Roelofs, M. B. J.; Sels, B. F.; De Vos, D. E. *Nat. Chem.* **2011**, 3, 382–387.
48. Abbaspourrad, A.; Carroll, N. J.; Kim, S. H.; Weitz, D. A., *Adv. Mater.* **2013**, 25, 3215–3221.
49. Yang Y.; Ambroggi, M.; Kirmse H.; Men Y. J.; Antonietti M., Yuan J. Y. *Chem. Mater.* **2015**, 27, 127–132.
50. Yang, H. Q.; Jiao, X.; Li, S. R. *Chem. Commun.* **2012**, 48, 11217–11219.
51. Zhang, X. M.; Zhao, Y. P.; Peng, J.; Yang, Q. H. *Green Chem.* **2015**, 17, 1899–1906.
52. Liu, J.; Yang, Q. H.; Zhang, L.; Yang, H. Q.; Gao, J. S.; Li, C. *Chem. Mater.* **2008**, 20, 4268–4275.
53. Liu, J.; Fan, F. T.; Feng, Z. C.; Zhang, L.; Bai, S. Y.; Yang, Q. H.; Li, C. *J. Phys. Chem. C* **2008**, 112, 16445–16451.
54. Aveyard, R.; Binks, B. P.; Clint, J. H. *Adv. Colloid Interface Sci.*, **2003**, 100–102, 503–546.
55. Qiao, Z. A.; Zhang, P. F.; Chai, S. H.; Chi, M. F.; Veith, G. M.; Gallego, N. C.; Kidder, M.; Dai, S. *J. Am. Chem. Soc.* **2014**, 136, 11260–11263.
56. Hashiguchi, S.; Fujii, A.; Takehara, J.; Ikariya, T.; Noyori, R. *J. Am. Chem. Soc.* **1995**, 117, 7562–7563.
57. Wu, X. F.; Li, X. G.; King, F.; Xiao, J. L. *Angew. Chem. Int. Ed.* **2005**, 44, 3407–3411.
58. Wu, X. F.; Vinci, D.; Ikariya, T.; Xiao, J. L. *Chem. Commun.* **2005**, 0, 4447–4449.
59. Li, X. G.; Wu, X. F.; Chen, W. P.; Hancock, F. E.; King, F.; Xiao, J. L. *Org. Lett.* **2004**, 6, 3321–3324.
60. Long, J.; Liu, G. H.; Cheng, T. Y.; Yao, H.; Qian, Q. Q.; Zhuang, J. L.; Gao, F.; Li, H. X. *J. Catal.* **2013**, 298, 41–50.
61. Deng, B. X.; Xiao, W.; Li, C. B.; Zhou, F.; Xia, X. L.; Cheng, T. Y.; Liu, G. H. *J. Catal.* **2014**, 320, 70–76.
62. Li, J. H.; Tang, Y. F.; Wang, Q. W.; Li, X. F.; Cun, L. F.; Zhang, X. M.; Zhu, J.; Li, L. C.; Deng, J. G. *J. Am. Chem. Soc.* **2012**, 134, 18522–18525.
63. Kong, L. Y.; Zhao, J. W.; Cheng, T. Y.; Lin, J. R.; Liu, G. H. *ACS Catal.* **2016**, 6, 2244–2249.
64. Chen, Z. J.; Guan, Z. H.; Li, M. R.; Yang, Q. H.; Li, C. *Angew. Chem. Int. Ed.* **2011**, 50, 4913–4917.
65. Sun, Q.; Jin, Y. Y.; Zhu, L. F.; Wang, L.; Meng, X. J.; Xiao, F. S. *Nano Today* **2013**, 8, 342–350.
66. Li, J.; Zhang, Y. M.; Han, D. F.; Gao, Q.; Li, C. *J. Mol. Catal. A: Chem.* **2009**, 298, 31–35.
67. Sun, Q.; Dai, Z. F.; Meng, X. J.; Wang, L.; Xiao, F. S. *ACS Catal.* **2015**, 5, 4556–4567.

TOC



A highly efficient and size-selective organic-inorganic hybrid microreactor with desired microenvironment was fabricated successfully for aqueous asymmetric catalysis.